Available online at www.sciencedirect.com

ScienceDirect

Procedia Engineering 203 (2017) 14–26

Procedia Engineering

www.elsevier.com/locate/procedia

26th International Meshing Roundtable, IMR26, 18-21 September 2017, Barcelona, Spain

A simple formula for quad mesh singularities

Harold J. Fogg[a], Liang Sun[b], Jonathan E. Makem[a], Cecil G. Armstrong[b], Trevor T. Robinson[b]

[a]*Meshing & Abstraction, Digital Factory, Simulation and Test Solutions Siemens PLM Software, SIEMENS, Francis House, 112 Hills Road, Cambridge, UK. CB2 1PH*

[b]*School of Mechanical and Aerospace Engineering, Queen's University Belfast, UK. BT9 5AH*

Abstract

A formula is presented for determining the net sum of mesh singularity indices that must occur in an all-quadrilateral (quad) mesh of a face or surface region after the mesh properties have been assigned on the face's boundaries and according to the face's Euler Characteristic. The formula is derived from Bunin's *Continuum Theory for Unstructured Mesh Generation* [1].

Peer-review under responsibility of the scientific committee of the 26th International Meshing Roundtable.

Keywords: all-quad mesh; singularities; cross-field

1. Introduction

Structured grids with tensor product structure offer numerical advantages over unstructured meshes. However, when it comes to closed surfaces we know from such familiar things as globes that sometimes singularities, where the regular grid structure is disrupted, are unavoidable. When the surface has boundaries forcing the grid to conform to them can also necessitate the introduction of singularities, not just to reduce the distortion of the grid, but there will be a certain minimum number that are essential for facilitating an all-quad mesh. How to determine the requisite mesh singularities based on the topological shape of the surface region and the geometric shapes of its boundaries will be covered in this paper.

1.1. Related work

A formula was proposed by White *et al.* [2] for determining if a face is submappable, which means that a *logical* representation can be found where all edges of the face are horizontal or vertical. First vertices are assigned types, which essentially decides the number of $\pi/2$ turns (signed with respect to an anticlockwise traversal) between the adjacent edges in a local logical representation. Values of 1, 0, -1 and -2 are assigned to *end*, *side*, *corner* and *reversal* vertices (*cf.* Fig. 1). If the sum of the vertex classification values is four it means that the local logical representations

[a] harry.fogg@siemens.com
[b] Liang.Sun@qub.ac.uk

1877-7058
Peer-review under responsibility of the scientific committee of the 26th International Meshing Roundtable.
10.1016/j.proeng.2017.09.781

of the vertices are consistent with a global logical representation for the face and thus the face is submappable. The check works on the principle that the sum of exterior angles at vertices of a planar polygon must equal 2π.

The formula was reformulated and generalised to multiply connected faces by Ruiz Girones *et al.* [3]. For the face to be submappable it must have assigned vertex types such that

$$E - C - 4R = 4(1 - H) \tag{1}$$

where E, C and R are the number of *end*, *corner* and *reversal* vertex types and H is the number of inner boundary loops.

Parametrisation-based mesh generation techniques have been intensely developed recently [4,5]. Their approach is to initialise and optimise a rotational symmetry vector field to improve its smoothness and in the process establish the number, indices and placements of mesh singularities. A secondary optimisation method solves for a parametrisation and hence mesh that fits with the rotational symmetry vector field. Ray *et al.* [6] and Knöppel *et al.* [7] prove the Poincaré-Hopf theorem on smooth and discrete closed oriented surfaces with empty boundaries which relates the net sum of singularity indices (defined slightly differently to here) to its Euler Characteristic.

1.2. Contributions

A new formula is presented which is equally simple but is more descriptive to that of Ruiz Girones *et al.*. It determines the net sum of mesh singularity indices that are required for a face, not just whether the face is submappable, and it accounts for general genera. The result is analogous to the Poincaré-Hopf theorem with the extension to non-empty boundaries on which alignment constraints are enforced. The particular case of four-way rotational symmetric direction (cross-) fields is specifically dealt with although the result could be extended to N-way rotational symmetric direction fields. The sufficiency of the formula for all-quad meshes is outlined.

2. Predicating theories

2.1. Euler Characteristic

If the face R is a regular (*i.e.* compact orientable) region of surface S its Euler Characteristic can be defined by

$$\chi(R) = V - E + F, \tag{2}$$

where V, E, F are the number of vertices, edges and facets of a triangulation (or a polygon mesh) on the face. The value does not depend on triangulation, hence it *characterises* the face [8, Prop. 1, Chp. 4.5]. The Euler Characteristic of a simple face R = disc can be ascertained by analysing a single triangle:

$$V = 3, E = 3, F = 1 \rightarrow \chi(\text{disc}) = 1. \tag{3}$$

The relationship between the genus, $g(S)$, and Euler Characteristic, $\chi(S)$, of a closed orientable surface with empty boundary S is

$$g(S) = \frac{2 - \chi(S)}{2} \tag{4}$$

[8, Prop. 4, Chp. 4.5]. The table to the right gives the genera and Euler Characteristics of familiar closed surfaces.

S	$g(S)$	$\chi(S)$
sphere	0	2
torus	1	0
double torus	2	-2
⋮	⋮	⋮

2.2. Global Gauss-Bonnet Theorem

The Global Gauss-Bonnet Theorem [8, Chp. 4.5] is

$$\sum_{i=1}^{N} \int_{C_i} \kappa_g(S)\, ds + \iint_R K(S)\, dA + \sum_{j=1}^{N} \gamma_j = 2\pi\chi(R) \tag{5}$$

where $C_1 \dots C_N$ are smooth regular curves embedded on the surface S that together form the boundary ∂R of the regular region R. Each C_i is positively oriented, *i.e.* the cross-product of the surface normal with a positive-sense-tangent ($\mathbf{n} \times \mathbf{t}$) points into the region. $\gamma_1 \dots \gamma_N$ are the set of all exterior angles at boundary vertices between the pairs of adjacent curves of $C_1 \dots C_N$. The internal angles θ_j are related to the exterior angles γ_j by

$$\theta_j = \pi - \gamma_j. \tag{6}$$

κ_g denotes the geodesic curvature of the curve C_i and K denotes the Gaussian curvature of the surface.

One insight to be made from Eqn. (5) is that by adding in an extra boundary closed loop made from a small circle whose radius $\to 0$, the LHS goes down by 2π and therefore the Euler Characteristic on the RHS must drop by 1. So, for a face R of a closed orientable surface S with genus $g(S)$ where the boundaries ∂R compose N loops, the Euler Characteristic of the face is

$$\chi(R) = \chi(S) - N, \tag{7}$$

$$= 2 - 2g(S) - N. \tag{8}$$

For example, a cylinder can be considered topologically to be a region of a sphere between two boundary loops, therefore,

$$\chi(\text{cylinder}) = 2 - 2 = 0. \tag{9}$$

2.3. A Continuum Theory for Unstructured Mesh Generation in Two Dimensions

Bunin [1] explains precisely a rigorous theory for a 'continuum description' of infinitesimal orthogonal quad meshes. Amongst other things, it explains the dependency of the number and indices of singularities that must occur on a face due to its intrinsic shape and boundary alignment constraints.

2.3.1. Definition

The continuum theory is derived in terms of a conformal mapping of a region (or face), R, with boundaries, ∂R, on a surface, S, to a region, $\tilde{R}$, of locally flat surface, $\tilde{S}$, with some conical vertices. The conformal mapping is encapsulated by a scalar field, ϕ, over the face. The flat surface must admit a family of orthogonal geodesics which encompass the images of the boundaries. This can be defined formally as a *ϕ-manifold* which is a Riemannian manifold with metric $\tilde{g}_{uv}$, defined on R with induced metric g_{uv} in $\mathbb{R}^3$, less a discrete set of points, P, such that:

1. g_{uv} is conformally related to $\tilde{g}_{uv}$, *i.e.* $g_{uv} = e^{2\phi}\tilde{g}_{uv}$, where $\phi \in \mathbb{R}$ on $R \backslash P$.
2. The ϕ-manifold is locally flat, *i.e.* its Gaussian curvature $\tilde{K} = 0$, on $R \backslash P$.
3. ϕ and $\nabla_s \phi$ are smooth and continuous on $R \backslash P$.
4. A cross-field (*i.e* a four-way rotational symmetry vector field [9]) with streamlines that are geodesics of $\tilde{g}_{uv}$ exists on $R \backslash P$.

The points in P correspond to the inverse images of cone vertices of $\tilde{g}_{uv}$ and also boundary vertices.

If the geodesics of the orthogonal family are chosen to describe a unit grid on the flat surface then its inverse image describes an isotropic orthogonal quad mesh. ϕ controls the isotropic stretching of the mapping and it can be intuitively thought of as the natural logarithm of the mesh refinement of the isotropic orthogonal quad mesh. Curvatures of mesh edges are related to variation in ϕ by

$$\kappa_g = \langle \nabla_s \phi, \mathbf{e} \rangle, \tag{10}$$

where κ_g denotes the geodesic curvature of the edge and its intrinsic normal, $\mathbf{e}$, is defined by $\mathbf{e} = \mathbf{n} \times \mathbf{t}$ where $\mathbf{n}$ and $\mathbf{t}$ are the surface normal and the edge tangent vector respectively.

2.3.2. Conditions

There are four conditions that ϕ must satisfy to constitute a valid continuum description.

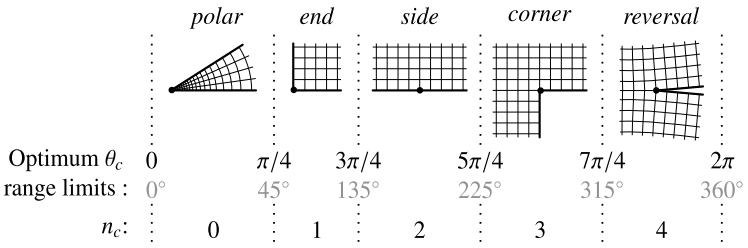

Fig. 1: Vertex classification.

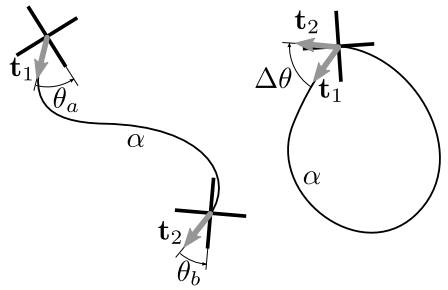

Fig. 2: Condition 4.

Condition 1. ϕ satisfies the Poisson equation over the face,

$$\Delta_s \phi = K + \sum_{i=1}^{M} k_i \frac{\pi}{2} \delta_{\mathbf{p}_i}, \quad k_i \in \mathbb{Z} \geq -4. \tag{11}$$

The source terms on the RHS are a distributed source for the Gaussian curvature and M point source terms at mesh singularities of strengths of $k_i\pi/2$, where the integer k_i is the singularity index. The point sources correspond to cone vertices of $\tilde{g}_{uv}$ with angle deficits of $k_i\pi/2$.

Condition 2. It follows from Eqn. (10) that for boundary alignment to be satisfied the flux across a boundary edge, $C_i \in \partial R$, must be

$$\kappa_g|_{C_i} = \langle \nabla_s \phi, \mathbf{e}_i \rangle, \tag{12}$$

where $\mathbf{e}_i$ is the intrinsic normal of the curve C_i.

Condition 3. At boundary vertices where the adjacent boundary curves are tangent discontinuous point sources necessarily occur. Their strength must satisfy

$$Q = 2\pi \left(n_c \frac{\pi/2}{\theta_c} - 1 \right) \tag{13}$$

which involves the corner angle, θ_c, and the predetermined vertex classification given by the integer n_c as shown in Fig. 1.

The optimum vertex classification that reduces the mesh distortion in the vicinity can be determined by minimising the source strength,

$$n_c|_{\text{optimum}} = \text{round}(\theta_c / \tfrac{\pi}{2}). \tag{14}$$

The optimum corner angle ranges for the different vertex types are given in Fig. 1.

Condition 4. Orthogonal geodesics of $\tilde{g}_{uv}$ can be described by the streamlines of a cross-field. It follows from Eqn. (10) that variation in the cross-field in one direction is controlled by flux in ϕ in a perpendicular direction. The condition is that for any smooth curve embedded on S, α, the total flux through the curve must induce a total turning angle of a cross that is multiple of $\pi/2$. Between two points a and b this is

$$\Phi_\alpha = \int_\alpha \langle \nabla_s \phi, \mathbf{e} \rangle \, ds = \int_\alpha \kappa_g \, ds + \theta_b - \theta_a + n\frac{\pi}{2}, \quad n \in \mathbb{Z}, \tag{15}$$

where are θ_a and θ_b are the angles (measured anticlockwise with respect to the local surface normal) between the initial and final curve tangents and one of the four vectors of the cross at those locations, as shown in Fig. 2 (left). For a closed curve the condition is

$$\Phi_\alpha = \oint_\alpha \langle \nabla_s \phi, \mathbf{e} \rangle \, ds = \oint_\alpha \kappa_g \, ds - \Delta\theta + n\frac{\pi}{2}, \quad n \in \mathbb{Z}, \tag{16}$$

where $\Delta\theta$ is the difference in angle of the initial and final curve tangents, as shown in Fig. 2 (right).

2.3.3. Solving the continuum description

Conditions 1–3 (Eqns. (11)–(13)) define a boundary value Poisson equation problem with Neumann boundary conditions (BCs) and distributed and point source loadings. An approximation of the exact solution of ϕ, which is smooth on $R \backslash P$ and unique up to an additive constant, can be found numerically by solving a linear system in a finite element analysis. However, the number of singularities, their indices and their positions need to be established first.

3. New formula

The main result of this paper is now given.

The net sum of the indices of M mesh singularities that occur in a boundary conforming all-quad mesh of a face R with genus $\chi(R)$ and prescribed vertex types $n_{c1} \ldots n_{cN}$ for the start vertices of boundary curves $C_1, \ldots C_N$ must satisfy

$$\sum_{i=1}^{M} k_i = -4\chi(R) + \sum_{j=1}^{N} \left(2 - n_{c_j}\right). \tag{17}$$

Proof. This can be proven straightforwardly by setting up a necessary condition from Bunin's Continuum Theory and simplifying it using the Gauss-Bonnet theorem.

3.1. Consistency flux balance condition

The Poisson equation describes steady-state fields, therefore over any subregion of the face the total flux of ϕ must balance in order for a solution to exist that satisfies Eqn. (11) in condition 1. Assessing the whole face the flux balance condition is

$$\Phi_{\partial R} + \Phi_R + \Phi_k = 0. \tag{18}$$

The total flux into the face through boundaries from curves and vertices is

$$\Phi_{\partial R} = \sum_{i=1}^{N} \int_{C_i} \kappa_g \, ds + \sum_{j=1}^{N} \left(\frac{\pi}{2} n_{c_j} - \theta_j\right), \tag{19}$$

where N is the number of curves and also the number of vertices. The total flux from the Gaussian curvature of the surface over the face is

$$\Phi_R = \iint_R K \, dA \tag{20}$$

and the total flux from the mesh singularities is

$$\Phi_k = \sum_{i=1}^{M} k_i \frac{\pi}{2}. \tag{21}$$

The consistency flux balance condition requires that

$$\Phi_{\partial R} + \Phi_R + \Phi_k = 0. \tag{22}$$

Equations (19) and (20) can be combined and simplified as follows:

$$\Phi_{\partial R} + \Phi_R = \sum_{i=1}^{N} \int_{C_i} \kappa_g \, ds + \iint_R K \, dA + \sum_{j=1}^{N} \left(\frac{\pi}{2} n_{c_j} - \theta_j \right), \tag{23}$$

$$= 2\pi\chi(R) - \sum_{j=1}^{N} \gamma_j + \sum_{j=1}^{N} \left(\frac{\pi}{2} n_{c_j} - \theta_j \right) \quad \ldots \text{Gauss-Bonnet, Eqn. (5)}, \tag{24}$$

$$= 2\pi\chi(R) - \sum_{j=1}^{N} (\pi - \theta_j) + \sum_{j=1}^{N} \left(\frac{\pi}{2} n_{c_j} - \theta_j \right) \quad \ldots \text{Eqn. (6)}, \tag{25}$$

$$= 2\pi\chi(R) - \sum_{j=1}^{N} \left(\pi - \frac{\pi}{2} n_{c_j} \right). \tag{26}$$

Then rearranging Eqn. (22) and substituting we get

$$-\Phi_k = \Phi_{\partial R} + \Phi_R, \tag{27}$$

$$-\sum_{i=1}^{M} k_i \frac{\pi}{2} = 2\pi\chi(R) - \sum_{j=1}^{N} \left(\pi - \frac{\pi}{2} n_{c_j} \right), \tag{28}$$

$$\sum_{i=1}^{M} k_i = -4\chi(R) + \sum_{j=1}^{N} \left(2 - n_{c_j} \right). \tag{29}$$

□

3.2. Examples

Examples and validations of the formula are given in Fig. 3 and Fig. 4. Red and blue dots mark singularities with indices -1 and 1 respectively. In Fig. 3 multiblock decompositions of a selection of sample faces are shown and their singularity index sums are demonstrated to agree with the resultants of the formula. In Fig. 4 two meshes of the same face are shown which were generated by a paving and multiblock decomposition method in Siemens Simcenter 3D [10]. The latter mesh has two vertex classification interpertations depending on whether the two nodes on the boundaries marked with blue dots are treated as singularities (VC1) or boundary vertices (VC2). The formula is shown to hold for both.

3.3. Relation to Ruiz Girones et al. check

Equation (17) can be shown to be equivalent to Eqn. (1) for topological discs. Using the variables in (1), the number of corners N and the total number of elements at the corners $\sum n_{c_i}$ can be expressed as

$$N = E + C + R, \quad \sum n_{c_i} = E + 3C + 4R. \tag{30}$$

From Eqn. (17)

$$\begin{aligned} \sum k_i &= -4\chi + 2(E + C + R) - (E + 3C + 4R) \\ &= E - C - 2R - 4\chi. \end{aligned} \tag{31}$$

For a topological disc with H inner boundary loops ($\chi = 1 - H$) and setting $\sum k_i = 0$, then

$$E - C - 2R = 4(1 - H). \tag{32}$$

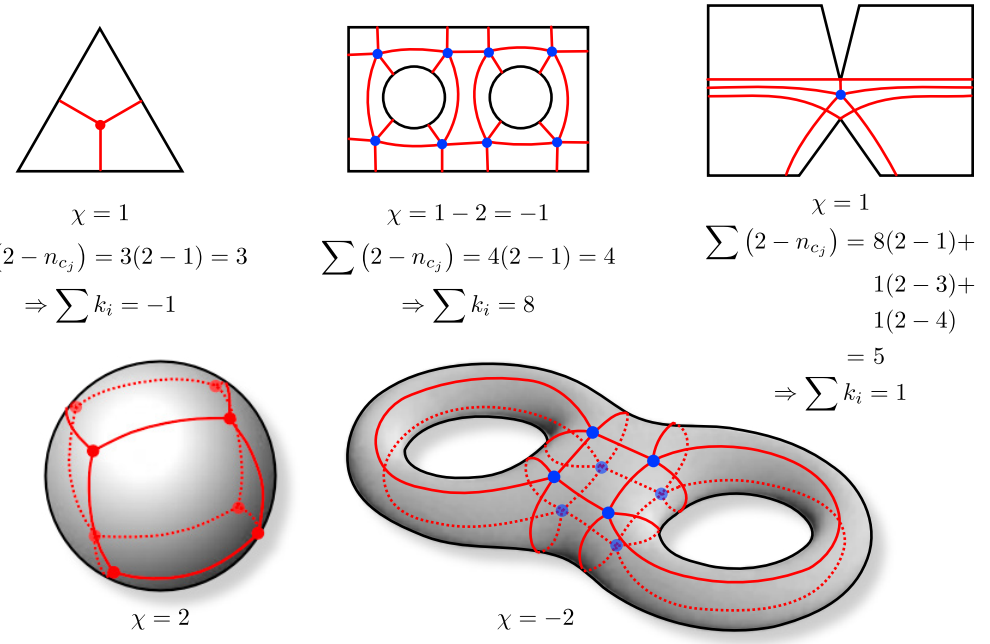

$\chi = 1$

$\sum (2 - n_{c_j}) = 3(2-1) = 3$

$\Rightarrow \sum k_i = -1$

$\chi = 1 - 2 = -1$

$\sum (2 - n_{c_j}) = 4(2-1) = 4$

$\Rightarrow \sum k_i = 8$

$\chi = 1$

$\sum (2 - n_{c_j}) = 8(2-1) + 1(2-3) + 1(2-4) = 5$

$\Rightarrow \sum k_i = 1$

$\chi = 2$

$\sum (2 - n_{c_j}) = 0$

$\Rightarrow \sum k_i = -8$

$\chi = -2$

$\sum (2 - n_{c_j}) = 0$

$\Rightarrow \sum k_i = 8$

Fig. 3: Some multiblock decompositions of surfaces and validation calculations of the formula.

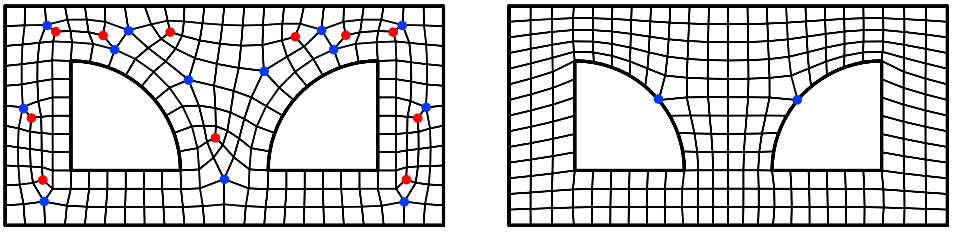

$\chi = -1$

Vertex classification 1 (VC1):

$\sum (2 - n_{c_j}) = 4(2-1) + 6(2-3) = -2$

$\Rightarrow \sum k_i = -4(-1) + (-2) = 2$

Sum of singularity indices:

$\sum k_i = 11(-1) + 13(1) = 2$ (VC1)

Vertex classification 2 (VC2):

$\sum (2 - n_{c_j}) = 4(2-1) + 8(2-3) = -4$

$\Rightarrow \sum k_i = -4(-1) + (-4) = 0$

Sum of singularity indices:

$\sum k_i = 2$ (VC1) or 0 (VC2)

Fig. 4: A paved mesh (left) and multiblock mesh (right) generated in Siemens Simcenter 3D [10]. Validiation calculations of the formula are given below.

4. Sufficiency of the formula

4.1. Satisfying condition 4

Any combination of singularities that result in a balanced total flux gives a well-posed Poisson equation problem with Neumann BCs that can be solved for a unique ϕ up to an additive constant, or equivalently a unique $\nabla_s \phi$ [11]. However, not all solutions satisfy condition 4.

4.1.1. Simply connected faces

On simply connected faces (i.e. topological discs and spheres) the $\nabla_s\phi$ solution satisfying conditions 1–3 automatically satisfies condition 4.

Proof. For a topological disc, R, with a single boundary loop composed of smooth boundary curves, C_i. Considering a subregion as illustrated in Fig. 5. The boundary is composed of $C_1, \dots C_N$ where the start and end curves C_1 and C_N are truncated by the points a and b, and these are joined by a non self-intersecting smooth curve α. The corner angles are labelled $\theta_{c_1} \dots \theta_{c_{N-1}}$ and θ_{c_a}, θ_{c_b}.

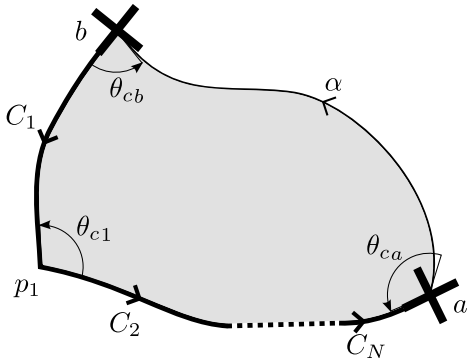

Fig. 5: Subregion, $\check{R}$, of simply connected face.

The Gauss Bonnet Theorem for the subregion is

$$\sum_{i=1}^{N}\int_{C_i}\kappa_g\,ds+\int_{\alpha}\kappa_g\,ds+\iint_{\check{R}}K\,dA+\sum_{i=1}^{N-1}(\pi-\theta_{ci})+(\pi-\theta_{ca})+(\pi-\theta_{cb})=2\pi \tag{33}$$

The flux balance condition on ϕ is

$$\Phi_{\partial\check{R}}+\Phi_{\check{R}}+\Phi_k=0. \tag{34}$$

The total flux over the subregion is

$$\Phi_{\check{R}}=\iint_{\check{R}}K\,dA. \tag{35}$$

The total flux though the boundaries is

$$\Phi_{\partial\check{R}}=\sum_{i=1}^{N}\int_{C_i}\kappa_g\,ds+\sum_{i=1}^{N-1}\left(\frac{\pi}{2}n_{c_i}-\theta_i\right)+\Phi_\alpha, \tag{36}$$

where Φ_α is the flux through α. The total flux from $\check{M}$ mesh singularities in the region is

$$\Phi_k=\sum_{j=1}^{\check{M}}k_j\frac{\pi}{2}. \tag{37}$$

Comparing Eqn. (33) and Eqns. (34), (35), (36) and (37)

$$-\int_{\alpha}\kappa_g\,ds+\Phi_\alpha+\sum_{i=1}^{N-1}\left(\frac{\pi}{2}(n_{c_i}-2)\right)=-\theta_{ca}-\theta_{cb}. \tag{38}$$

With respect to the definition of Condition 4, $\theta_a=\theta_{ca}$ and $\theta_b=\pi/2-\theta_{cb}$. Therefore,

$$\Phi_\alpha=\int_{\alpha}\kappa_g\,ds+\theta_b-\theta_a\underbrace{-\frac{\pi}{2}-\sum_{i=1}^{N-1}\left(\frac{\pi}{2}(n_{c_i}-2)\right)-\sum_{j=1}^{\check{M}}k_j\frac{\pi}{2}}_{n\frac{\pi}{2}\,|\,n\in\mathbb{Z}} \tag{39}$$

□

which proves that the flux through α always satisfies Condition 4.

The more simple analogous analysis for a topological sphere with empty boundary gives the same result.

4.1.2. Multiply connected surfaces

For multiply connected surfaces the total flux to satisfy condition 4 must be enforced between separate boundary closed loops and around surface handles. This can be achieved by creating cuts until a simply connected face is produced where the cuts appear twice with opposite senses in its boundary closed loops and Neumann BCs are applied across the cuts so as to satisfy the required total flux. In a finite element analysis the BCs that minimise the Dirichlet energy, $\int_R \|\nabla_s \phi\|^2 \, dA$, may be found as part of the solution by using multiple point constraints to enforce the total fluxes across the cuts. However, the $\nabla_s \phi$ solution (that is unique for the applied BCs) may not allow for a corresponding continuous ϕ to exist.

4.2. Integrability

The behaviour of a cross-field is governed by the surface gradient of ϕ. Considering the unknown to be $\mathbf{v} \coloneqq \nabla_s \phi$, Eqn. (11) becomes

$$\nabla_s \cdot \mathbf{v} = K + \sum_{i=1}^{M} k_i \frac{\pi}{2} \delta_{\mathbf{p}_i}, \quad k_i \in \mathbb{Z} \geq -4. \tag{40}$$

A unique cross-field comes from a continuous (on $R \backslash P$) $\mathbf{v}$ once a cross orientation at one point is set.

Helmholtz theorem states that any vector field can be decomposed into the gradient of a *scalar potential* and the curl of a *vector potential*. Therefore $\mathbf{v}$ is irrotational from its definition. It follows that $\mathbf{v}$ is *locally integrable* which means that over any simply connected subregion, $\breve{R}$:

1. ϕ (C^1 on $\breve{R} \backslash P$) can be found such that $\mathbf{v} = \nabla_s \phi$.
2. The circulation around the simple closed path perimeter is zero, $\oint_{\partial \breve{R}} \langle \mathbf{v}, \mathbf{t} \rangle \, ds = 0$

If these are true over all (multiply connected or not) subregions then $\mathbf{v}$ is *globally integrable*. In that case a continuous on $R \backslash P$ cross-field, ϕ and corresponding isotropic mesh can all be found. But this is not the case in general.

Since $\mathbf{v}$ does not define the directions of cross-field streamlines but the maximal rate of change of angle of the cross-field, $\mathbf{v}$ solutions with circulation can have corresponding cross-fields that admit orthogonal (anisotropic) quad meshes so long as cross-field streamlines don't spiral. Spiralling occurs when,

$$\oint_\alpha \langle \mathbf{v}, \mathbf{t} \rangle \, ds \neq 0 \quad \text{and}$$
$$\oint_\alpha \langle \mathbf{v}, \mathbf{e} \rangle \, ds = \oint_\alpha \kappa_g \, ds - \Delta\theta. \tag{41}$$

That is, when $n = 0$ in Eqn. (16) for a closed curve with a non-zero circulation of $\mathbf{v}$.

A simple example is shown in Fig. 6 where a square face has a rotated square hole. Condition 4 forces a total flux to occur between the outer and inner boundary loops. A continuous $\mathbf{v}$ solution can be found satisfying these flux conditions but it is not globally integrable due to the circulation of $\mathbf{v}$ around the hole, and therefore it cannot be integrated to give a continuous ϕ solution. The ϕ solution shown (Fig. 6 (left)) has a discontinuous step change across the cut where condition 4 is imposed. The streamlines of the the associated cross-field to $\mathbf{v}$ (Fig. 6 (centre)) do not spiral as $n = 4$ (plus-minus depending on traversal direction) in Eqn. (16) for a closed path around the hole. Therefore the cross-field admits an orthogonal (anisotropic) quad mesh (Fig. 6 (right)) despite the global non-integrability of $\mathbf{v}$.

A counterpoint example where a cross-field of a continuous globally non-integrable $\mathbf{v}$ does not admit a quad mesh is the *nautilus* face shown in Fig. 7. The circulation of $\mathbf{v}$ for all closed curves around the hole cannot be zero due to Condition 4, which prevents the existence of a continuous ϕ. The streamlines clearly spiral as indicated which prevents the existence of a corresponding orthogonal quad mesh.

The disc face in Fig. 8 has continuous $\mathbf{v}$, ϕ and cross-field solutions and thus a corresponding isotropic quad mesh is realisable. Condition 4 allows the circulation around the hole to be zero and therefore despite having $n = 0$ in Eqn. (41) for a closed curve around the hole the streamlines do not spiral but close onto themselves.

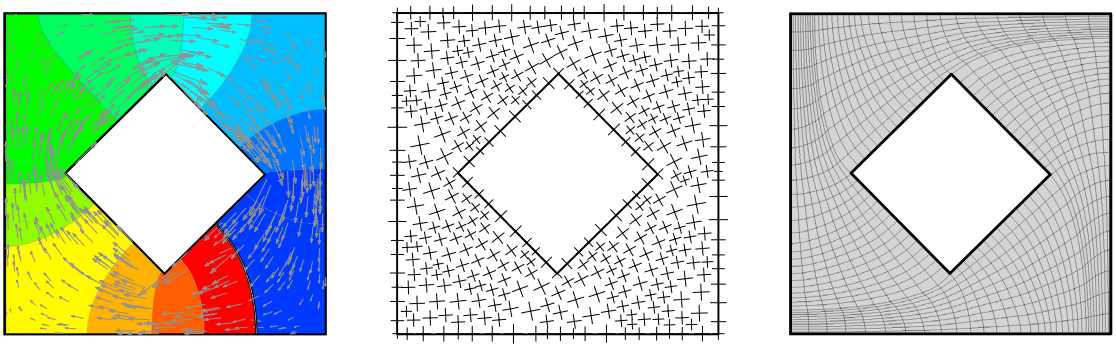

Fig. 6: Square face with a rotated square hole. Continuous $\mathbf{v}$ and discontinuous ϕ solutions (left), related boundary-aligned cross-field (centre) and corresponding orthogonal quad mesh (right).

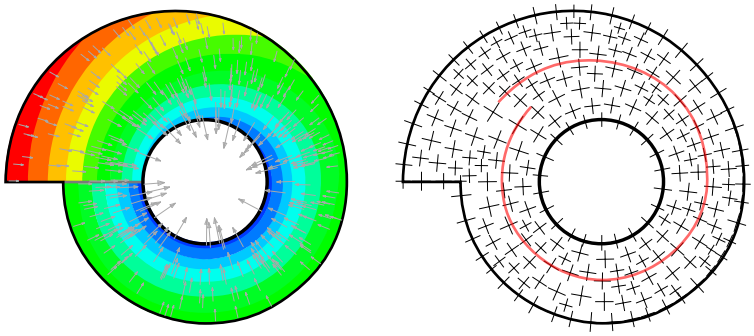

Fig. 7: Continuous $\mathbf{v}$, discontinuous ϕ, cross-field and spiralling streamline on *nautilus* face.

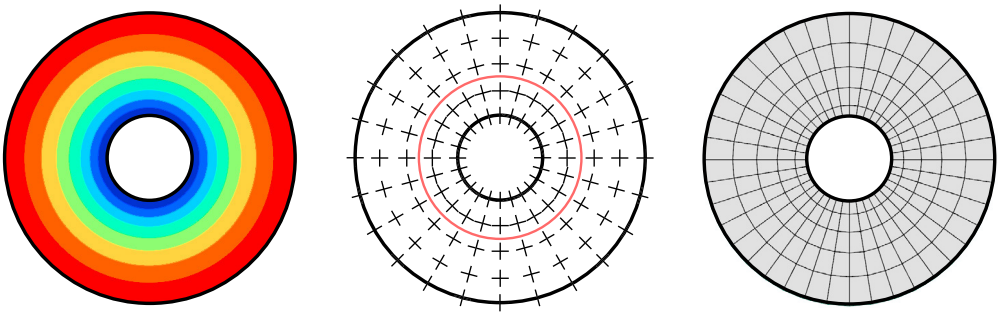

Fig. 8: Continuous ϕ, cross-field and loop streamline on disc face.

4.3. Sufficiency summary

The formula is a necessary but not sufficient condition for the possible mesh singularities that occur in a boundary conforming all-quad mesh of a face. The formula allows for an indefinite number of singularity combinations that meet the flux balance condition. For each of these singularity combinations a continuous (on $R\backslash P$) $\mathbf{v} := \nabla_s \phi$ vector field exists that satisfies the continuum description conditions 1–4. It is unique for simply connected faces but not for multiply connected faces. A corresponding cross-field exists for a $\mathbf{v}$ solution. If $\mathbf{v}$ is globally integrable then a corresponding continuous ϕ exists for which all-quad meshes are compatible. If $\mathbf{v}$ is not globally integrable, which can only happen for multiply connected faces, a corresponding continuous ϕ does not exists but the cross-field may still be compatible with an all-quad mesh if spiralling of cross-field streamlines does not occur.

4.4. Non-orthogonal cross-fields

Bunin's theory applies to orthogonal cross-fields but it has been shown that general non-orthogonal *4-PolyVector* fields can be represented by orthogonal cross-fields [12]. The basic idea is that the bisectors of skewed 4-PolyVector directions form an orthogonal cross-field with the usual singularities. This implies that non-orthogonal 4-PolyVector-fields do not involve more complex behaviour than cross-fields and the rules and constraints that apply to cross-fields also apply to general non-orthogonal 4-PolyVector fields.

5. Potential applications

5.1. Identifying sweepable volumes

White *et al.* [13] have used Eqn. (1) to identify sweepable volumes, including those that can be meshed with one-to-one, one-to-many, many-to-many sweeping algorithms. For sweepable volumes the 2-D quad meshes on the source faces are swept through the volume to the target faces. This will produce a structured quad mesh on the linking faces between the source and target faces. Therefore, by identifying loops of faces which can be structured meshed and by evaluating the angles at the edges, a volume can be classified as sweepable or non-sweepable. The sweeping paths of the above mentioned sweepable volumes are all open curves. An extension of using Eqn. (17) as opposed to (1) is that a volume can be identified as being suitable for sweep meshing where the mesh is formed by sweeping a surface mesh along a smooth closed curve (including those formed by revolving around an axis). The feature of this type of sweepable volume is that each face has zero mesh singularities with $\chi = 0$ and $\sum(2 - n_{c_i}) = 0$, as shown in Fig. 9 (a). This differs from a submappable volume where each face also has zero mesh singularities but with $\chi = 1$ and $\sum(2 - n_{c_i}) = 4$, as shown in Fig. 9 (b).

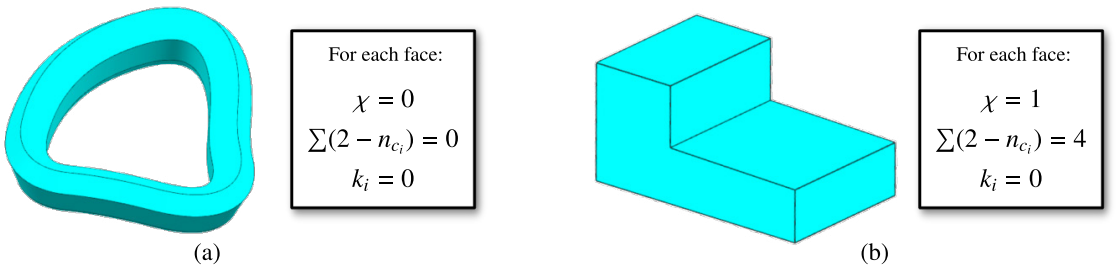

Fig. 9: (a) sweepable volume where the sweeping path is a smooth and closed curve; (b) submappable volume.

5.2. Locating mesh singularities

Equation (17) shows that the net sum of the singularities is determined by the Euler Characteristic, χ, and the number of elements at each corner. Suppose a small offset is made to the boundaries of a surface as shown in Fig. 10. If the number of mesh singularities does not change for the surface after offset S_3, then it can be claimed the net

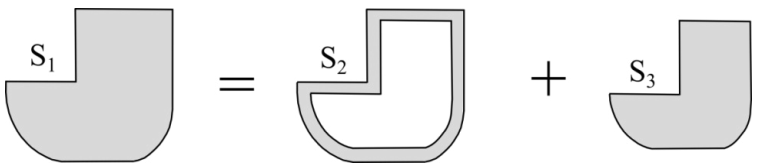

Fig. 10: Making an offset of the boundaries of the original surface.

number of mesh singularities in the offset surface S_2 is zero (S_2 has no mesh singularities or pairs of positive and negative singularities). If the number of mesh singularities in S_1 and S_3 is different, a mesh singularity should appear

in S_2. A reasonable place to locate the singularity is in the region of the corner where the number of elements or the Euler Characteristic changes. The offset operation can be made until the shape after offset is small and the number of mesh singularities stops varying. Therefore, by making the offset of the boundaries inwards and tracing the change of the element number or Euler Characteristic at each corner, the singularities can be located.

Fig. 11 (a) shows a squeezed rectangle with a net number of zero mesh singularities. The net number changes from

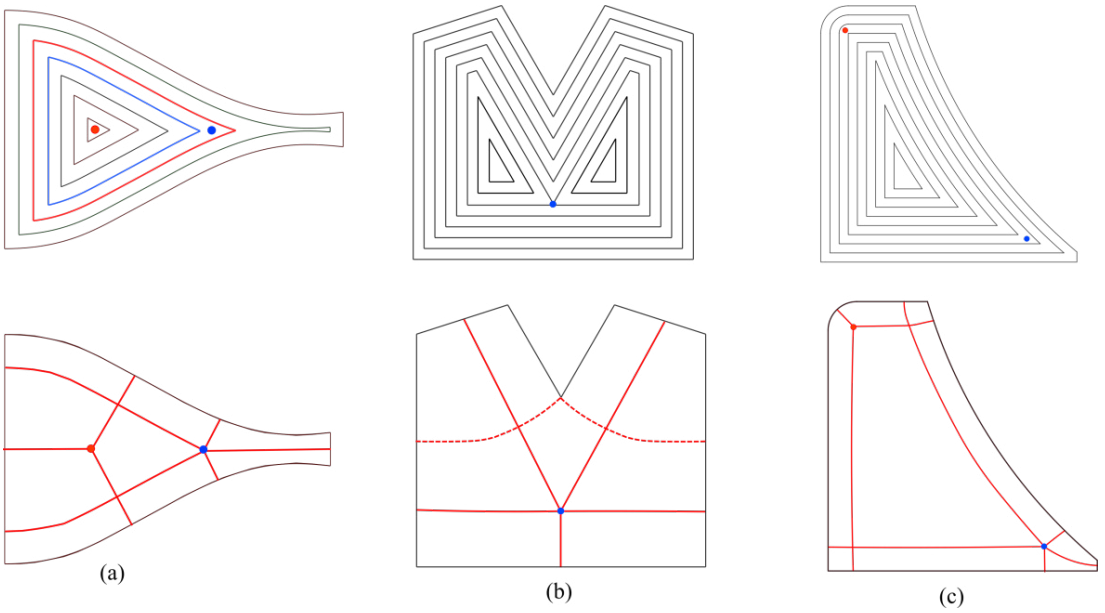

Fig. 11: Examples of locating mesh singularities using offsets: (a) the element number at the corner changes; (b) the Euler Characteristic changes; (c) a pair of positive and negative mesh singularities within one offset. Split lines from the singularities are shown in solid red lines and other split lines are shown in dashed red.

0 to 1 when offsetting from the red contour to the blue contour. This is caused by the angle of the rightmost corner passing though 45° and its vertex type switching from $n_c = 0$ to $n_c = 1$. Therefore, a positive mesh singularity can be placed between the blue and red lines in the region of the right corner. With further offsets, the shape becomes a triangle and the element number does not change any more. For a triangle with one element at each corner, one negative singularity is required, as the red point shows. Fig. 11 (b) shows an example where the Euler Characteristic changes during the offset process. There is one positive singularity for the original shape. When it offsets to the position as shown the original shape becomes two separate shapes with zero mesh singularities. Therefore the positive singularity will be placed at the transition position. In principle, the offset distance needs to be small. But it is still possible that a pair of positive and negative singularities exist within one offset, as shown in Fig. 11 (c). However, by checking whether the number of elements or the Euler Characteristic changes at each corner of the offset geometry, the positive and negative singularities can still be properly located. Examples of the manual block decomposition are given in the second row in Fig. 11. In fact, the offset boundaries offer some clues for the decomposition lines, *e.g.* some lines follow the offset boundaries and some others are roughly perpendicular to them. The construction of these partitioning lines is not the focus here and will not be discussed in detail, but is an interesting avenue for further research.

With the offsetting boundary method it is also possible to locate the singularity lines in 3-D for hex meshing. An equivalent equation to (17) in 3-D will be required and also a routine to determine the required number of elements at each corner. The model in Fig. 12 demonstrates an initial guess. The model is a cube with three equal blends, Fig. 12 (a). Fig. 12 (b) shows the result after the first offset. Evidently there will be no singularities in the region between Fig. 12 (a) and Fig. 12 (b). However, after the second offset, Fig. 12 (c), the number of singularities on the bounding surfaces has changed. This means that the singularity occurs between Fig. 12 (b) and Fig. 12 (c). It is necessary to conduct further research to formulate the detailed rules for the placement of singularity lines following this approach.

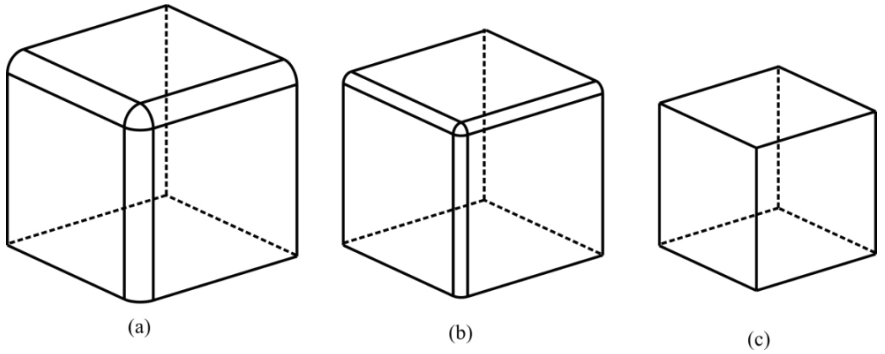

Fig. 12: A 3-D example of locating the singularity lines by offsetting the boundaries.

6. Conclusion

A proof of a simple formula for the possible combinations of mesh singularities in a boundary conformal all-quad mesh on a face has been presented. The only parameters involved are the vertex types for the quad mesh and the Euler Characteristic of the face. Its sufficiency has also been discussed. The use of the formula has been demonstrated on a range of faces to provide an intuitive validation of its correctness. Some potential applications were briefly discussed on the identification of sweepable volumes and building singularity line networks in all-hex meshes by an offsetting approach.

Acknowledgements

The authors from the Meshing and Abstraction Group, Simcenter, Siemens PLM would like to thank their manager Mary Otte for her support and encouragement in doing this work. The authors from Queen's University Belfast would like to acknowledge the financial support provided by Innovate UK, a UK Centre for Aerodynamics project, via GHandI project (TSB 101372).

References

[1] G. Bunin, A continuum theory for unstructured mesh generation in two dimensions, Comput. Aided Geom. Des. 25 (1) (2008) 14–40.
[2] D. White, L. Mingwu, S. E. Benzley, G. D. Sjaardema, Automated hexahedral mesh generation by virtual decomposition, in: Proceedings of the 4th International Meshing Roundtable, Sandia National Laboratories, 1995, pp. 165–176.
[3] E. Ruiz-Girones, J. Sarrate, Generation of structured meshes in multiply connected surfaces using submapping, Advances in Engineering Software 41 (2) (2010) 379 – 387. doi:10.1016/j.advengsoft.2009.06.009.
[4] D. Bommes, B. Lvy, N. Pietroni, E. Puppo, C. S. a, M. Tarini, D. Zorin, State of the art in quad meshing, in: Eurographics STARS, 2012.
[5] A. Vaxman, M. Campen, O. Diamanti, D. Panozzo, D. Bommes, K. Hildebrandt, M. Ben-Chen, Directional Field Synthesis, Design, and Processing, Computer Graphics Forumdoi:10.1111/cgf.12864.
[6] N. Ray, B. Vallet, W. C. Li, B. Lévy, N-symmetry direction field design, ACM Trans. Graph. 27 (2) (2008) 10:1–10:13. doi:10.1145/1356682.1356683.
[7] F. Knöppel, K. Crane, U. Pinkall, P. Schröder, Globally optimal direction fields, ACM Trans. Graph. 32 (4) (2013) 59:1–59:10. doi:10.1145/2461912.2462005.
[8] M. P. do Carmo, Differential Geometry of Curves and Surfaces, 1st Edition, Pearson, 1976.
[9] J. Palacios, E. Zhang, Rotational symmetry field design on surfaces, ACM Trans. Graph. 26 (3). doi:10.1145/1276377.1276446.
[10] Siemens Simcenter 3D, www.plm.automation.siemens.com/en_us/products/simcenter/3d/modeling/index.shtml, (26-May-2017).
[11] J. Jackson, Classical electrodynamics, Wiley, New York, 1999.
[12] O. Diamanti, A. Vaxman, D. Panozzo, O. Sorkine-Hornung, Designing n-polyvector fields with complex polynomials, Comput. Graph. Forum 33 (5) (2014) 1–11. doi:10.1111/cgf.12426.
[13] D. R. White, T. J. Tautges, Automatic scheme selection for toolkit hex meshing, International Journal for Numerical Methods in Engineering 49 (1-2) (2000) 127–144. doi:10.1002/1097-0207(20000910/20)49:1/2<127::AID-NME926>3.0.CO;2-V.